Biophysical Journal
Article

Biophysical Society

Mode of Action of Antimicrobial Peptides on *E. coli* Spheroplasts

Yen Sun,[1] Tzu-Lin Sun,[1] and Huey W. Huang[1,*]
[1]Department of Physics & Astronomy, Rice University, Houston, Texas

ABSTRACT We investigated the phenomena of antimicrobial peptides (AMPs) directly attacking the cytoplasmic membranes of *Escherichia coli* spheroplasts. We developed a procedure for fluorescence recovery after photobleaching to examine dye leakage through bacterial membranes as AMPs in solution bound to the membranes. We found that the AMP binding did not increase the apparent membrane area of a spheroplast, contrary to the response of a lipid-bilayer vesicle, which always showed a membrane area expansion by AMP binding. The permeability through the bacterial membrane increased in a sigmoidal fashion as the AMP binding increased in time, exhibiting a cooperative behavior of AMPs. The analysis of fluorescence recovery after photobleaching showed that the fluxes of dye molecules into and out of the cell were consistent with diffusion of molecules through a number of pores that increased with binding of AMPs and then saturated to a steady level. We discovered a new, to our knowledge, experimental parameter called the flux rate that characterizes the AMP-induced permeability of dye molecules through bacterial membranes. The phenomena observed in bacterial membranes are consistent with the pore-forming activities of AMPs previously observed in lipid bilayers. The experimental value of the flux rate per pore is much smaller than a theoretical value that assumes no friction for the dye molecule's permeation through the pore. We believe that experimental studies of the flux rate will be useful for further analysis of AMPs' permeabilization mechanisms.

INTRODUCTION

Host-defense antimicrobial peptides (AMPs) were first discovered in the early 1980s and subsequently found in almost every organism (1–5). Initially, the discoverers and pioneers of the field had to wrestle with questions about the molecular targets of these antibiotics (1–5). By the late 1980s, accumulated evidence, especially an experimental result showing that the natural all-L peptides and their D enantiomers were equally active (4), convincingly showed that the main targets of AMPs are bacterial cytoplasmic membranes, rather than stereospecific molecular receptors (5). Since then, investigators have sought to answer the major question regarding AMPs: what are their molecular mechanisms in bacterial cytoplasmic membranes? Some studies attempted to address this issue using live bacteria (3,6–9). However, bacterial studies are limited by the methods that can be used, complicated by both the presence of outer membranes (6) and the fact that the action of antimicrobials can induce secondary effects, including activation of autodigestive enzymes resulting in cell membrane lysis (10,11).

Perhaps for this reason, studies of AMPs have mostly been performed with model membranes or lipid bilayers. Thus, there are persistent questions as to whether the action of AMPs on artificial membranes can be reproduced with bacterial membranes, and whether one can extend the results of model membranes to bacterial membranes (12). The mechanism of AMPs is the basis for understanding their efficacy, toxicity, and bacterial resistance. A well-understood membrane permeabilization mechanism is also potentially useful for drug and gene delivery.

In this study, we investigated the action of AMPs on *Escherichia coli* spheroplasts from which the outer membranes had been removed. The removal of the outer membrane made it possible to observe the action of AMPs on the cytoplasmic membranes. In preparation for this study, we previously investigated the physical properties of spheroplast membranes by using the micropipette aspiration method (13). We found that the properties of bacterial cell membranes are dominated by the existence of a membrane reservoir (e.g., membrane folds), and thus are significantly different from those of a lipid-bilayer vesicle made of bacterial lipid extract (13). Furthermore, we found that these characteristic properties of bacterial membranes are metabolically maintained. Therefore, we were very curious to know how the actions of AMPs on

Submitted March 7, 2016, and accepted for publication May 25, 2016.
*Correspondence: hwhuang@rice.edu
Editor: Paulo Almeida.
http://dx.doi.org/10.1016/j.bpj.2016.05.037

spheroplast membranes would compare with the actions on lipid bilayers.

We studied the actions of human AMP LL-37 (14) and bee venom toxin melittin (15) on *E. coli* spheroplasts by using the micropipette aspiration method. It is very important to note that we studied the effect of AMPs in the micromolar range of concentration. This is the range of concentration in which the antibacterial activities of AMPs, including the minimal inhibitory concentrations, were previously measured (5,16). The interaction of AMPs with lipid bilayers is strongly concentration dependent, and the phenomena of AMPs may look different at much lower or much higher concentrations (17). We developed a procedure for fluorescence recovery after photobleaching (FRAP) to examine dye leakage through bacterial membranes as AMPs in solution bound to the membranes. We found a new, to our knowledge, experimental parameter called the flux rate that characterizes the AMP-induced permeability of dye molecules through a membrane. We believe that this parameter is potentially useful for in-depth studies of AMP mechanisms.

MATERIALS AND METHODS

Bacterial strains and culture

The *E. coli* K-12 strain MG1655 (ATCC 700926) was purchased from ATCC (Manassas, VA). Luria-Bertani medium (5 g/L yeast extract, 10 g/L peptone from casein, and 10 g/L sodium chloride; EMD Millipore, Billerica, MA) containing 15 g/L agar (EMD) was used for the growth of colonies of *E. coli*. To ensure sterility, the medium was autoclaved before use.

Chemicals and media

Sucrose, glucose, Tris, hydrochloric acid, lysozyme, DNase, EDTA, magnesium chloride, sodium hydroxide, cephalexin, and carboxyfluorescein were purchased from Sigma Aldrich (St. Louis, MO). Texas Red sulfonyl chloride (TRsc, molecular weight 625) and calcein (molecular weight 623) were purchased from Invitrogen (Grand Island, NY).

Preparation of *E. coli* spheroplasts

We prepared giant spheroplasts of *E. coli* (13) by following the detailed procedure described by Renner and Weibel (18). Briefly, cells were grown in Luria-Bertani medium. To grow long filamentous cells, cephalexin (60 μg/mL) was added. After the cells reached an average length of ~50 μm, they were harvested. Spheroplasts from filamentous cells were formed by adding reagents in the following order: 30 μL 1 M Tris•HCl (pH 8.0), 24 μL 0.5 mg/mL lysozyme, 6 μL 5 mg/mL DNase, and 6 μL 125 mM EDTA-NaOH (pH 8.0). After 5–20 min at room temperature, 100 μL of STOP solution (10 mM Tris•HCl at pH 8, 0.7 M sucrose, 20 mM $MgCl_2$) was added to stabilize the spheroplasts. The spheroplasts were stored in liquid nitrogen for no longer than 2 weeks. Frozen spheroplasts were thawed slowly on ice before each use. Then, 30 μL of spheroplasts was injected into an observation chamber containing STOP solution at 0.338 osmole/kg osmolality.

Method of micropipette aspiration

The method used for micropipette aspiration was a modification of the original method of Kwok and Evans (19) as described in Sun et al. (20,21). A micropipette was connected to a water-filled U tube manometer and a negative pressure in the pipette was produced by adjusting the height of the water level with reference to the atmosphere pressure (20). Although the same technique is used to measure spheroplasts and giant unilamellar vesicles (GUVs), the small size of the spheroplasts imposes some restrictions on spheroplast measurements. The technical details of the micropipette aspiration experiment on *E. coli* spheroplasts were described in (13).

RESULTS

Spheroplasts attacked by LL37 and melittin

In our previous study (13) we established a procedure for producing and maintaining *E. coli* spheroplasts in a range of osmolalities. In general, the average size of the cells increased with decreasing osmolality, but in all cases the spheroplast membranes were without a surface tension, unless the spheroplast was extremely swollen (13). Nonetheless, if a spheroplast was subjected to an aspiration pressure, a surface tension would develop reversibly with the applied suction pressure (13). For the experiment described here, we let spheroplasts equilibrate in 0.338 osmole/kg (Osm), from which we transferred a small number of cells, ~5 μm in diameter and tensionless, to an observation chamber that contained calcein at 60 μM. A micropipette equipped with an adjustable sucking pressure via a water column was used to hold a spheroplast at a pressure that produced a very small membrane tension, $<$0.25 mN/m (13). The purpose of the micropipette aspiration was to hold the cell in position for confocal imaging and for monitoring possible membrane area changes (13).

At time zero, an open pipe (120 μm in diameter) containing LL37 at 6 μM was introduced into the observation chamber to let LL37 diffuse to the spheroplast (the distance from the opening of the pipe to spheroplast was ~30–40 μm). We monitored the protrusion length of the spheroplast into the aspiration micropipette, which would report on the membrane area change of the spheroplast (13), and the fluorescence intensity of calcein in a region including both inside and outside of the spheroplast. A typical run of such an experiment produced the following result (Fig. 1): before the introduction of LL37, there was no leakage of calcein into the spheroplast. After the introduction of LL37, the fluorescence intensity of calcein inside the spheroplast increased in a sigmoidal fashion to a steady value (i.e., a plateau). Then the fluorescence intensity might suddenly jump to the same intensity as observed outside. When that happened, the phase contrast of the cell interior was also lost. The spheroplasts typically lasted ~40 min or longer without losing their phase contrast while being subjected to the attack of LL37. As such, we generally limited our experiment to ~40 min. In all cases, no membrane area changes were detected. Fig. 1 shows the confocal images of

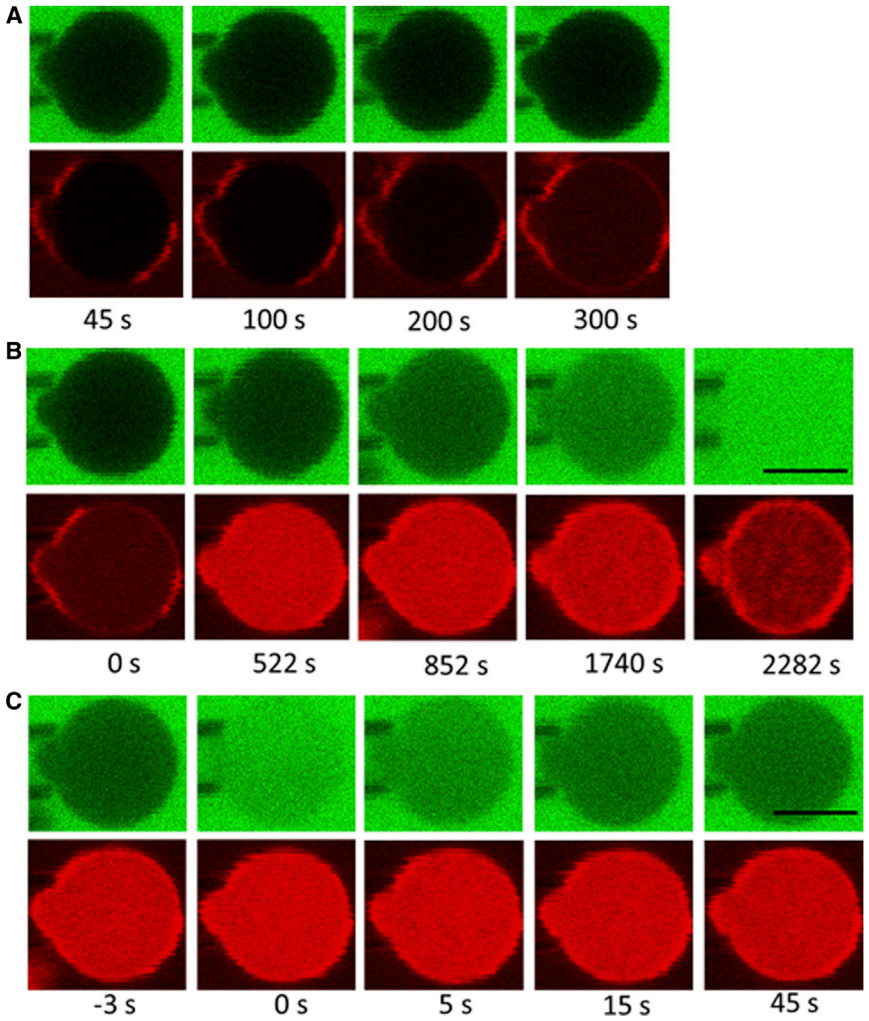

FIGURE 1 Confocal images of a micropipette-aspirated spheroplast during the experiment, in both green (calcein) and red (TRsc) channels. Scale bar, 5 μm. (*A*) The spheroplast was in a solution containing calcein at 60 μM for detecting leakage into the cell and TRsc at 40 μM for marking the boundary of the spheroplast so as to measure any possible membrane area changes. TRsc is a protein-labeling dye that can spontaneously permeate through the membrane. No leakage of calcein was detected in the absence of AMPs. (*B*) At time zero, an open pipe containing LL37 at 6 μM was introduced close to the spheroplast. Thereafter, the green fluorescence intensity inside the cell sigmoidally increased to a steady state. At 2282 s, the inside green fluorescence abruptly increased to the same intensity as observed outside. (*C*) One of many FRAP experiments performed during (*B*). After a dark period from -3 to 0 s, the intracellular green fluorescence intensity decayed from a high value back to a level close to the intensity right before the dark period (at-3 s). The confocal scanning time for each image was 0.5 s.

the spheroplast during one run of such experiments. The protein-labeling dye TRsc (22) at 40 μM in solution was used to mark the boundary of the spheroplast for the purpose of measuring possible membrane area changes. Note that TRsc spontaneously permeated through the membrane before the introduction of LL37, when no leakage of calcein was detected.

Melittin produced effects similar to those observed for LL37. Qualitatively, there was no difference between the results obtained with melittin and LL37.

FRAP experiment on spheroplasts

The light that excited the fluorescent dye calcein also photobleached a fraction of the dye molecules per unit time. A steady state of fluorescence intensity within the spheroplast was possible only if unbleached dye molecules diffused into the cell to replace the bleached dye molecules. If the incident light for fluorescence was blocked for a time, the fluorescence intensity outside the spheroplast did not change when the fluorescence measurement resumed. This was because the dye molecules outside the cell mixed rapidly with unbleached dye molecules beyond the lighted region. As a result, the concentration of bleached dye molecules outside the spheroplast was constantly diluted to a negligible level, so the fluorescence intensity outside the cell was constant in time. The fluorescence intensity inside the cell was different. The exchange of dye molecules between inside and outside of the cell was slower than free diffusion. There was always a significant concentration of bleached dye molecules inside the cell, which is why the fluorescent intensity during the steady state was lower than that of the outside solution. After a dark period, the fluorescence intensity within the spheroplast increased because unbleached dye molecules had entered the spheroplast from outside to replace the bleached dye molecules inside during the dark period. Phenomenologically, we can describe the time (t) dependence of the unbleached calcein concentration $C(t)$ inside a spheroplast as follows:

During the fluorescence measurement, the concentration $C(t)$ is reduced at the rate of $(1/\tau)C(t)$ due to photobleaching. Imagine that the spheroplast membrane has pores and

the molecules diffuse into and out of the cell through these pores. The influx (in molecules per second) through a circular pore of radius a is given by the Berg-Purcell formula $4aDC_{out}$ (23), where D is the diffusion constant of the dye molecule and C_{out} is the unbleached dye concentration outside the cell. Thus, if the total number of pores is N, the total dye influx is $4aDNC_{out} \equiv j_c C_{out}$. If V is the volume within the spheroplast that is accessible to the dye molecules, the influx will increase the dye concentration per unit time by $(j_c/V)C_{out}$. Similarly, the outflux of unbleached dye from within the cell is $j_c C(t)$. The kinetics of the unbleached dye concentration inside the spheroplast is then given by

$$\frac{dC(t)}{dt} = -\frac{1}{\tau}C(t) - \frac{j_c}{V}C(t) + \frac{j_c}{V}C_{out}. \quad (1)$$

Although there is a theoretical formula for j_c, it should be regarded as an experimental parameter. Thus, this equation contains two unknown quantities: the photobleaching time constant τ and the flux rate j_c. The value of τ depends on the instrumentation. The flux rate j_c is characteristic of the permeability induced by the AMP. Both quantities are measurable by the FRAP experiment.

During a steady state, $dC(t)/dt = 0$, $C(t) \rightarrow C_s$. The flux rate j_c is a constant that satisfies the relation $C_s/\tau_e = j_c C_{out}/V$, with $1/\tau_e = 1/\tau + j_c/V$. The photobleaching is balanced by the net influx of unbleached dye molecules. When we blocked the incident light for a short time, the absence of photobleaching increased $C(t)$ to a value C_i greater than C_s. When we turned on the light again for measurements, $C(t)$ would decay from C_i back to C_s following the relation $C(t) - C_s = (C_i - C_s)e^{-t/\tau_e}$. Thus, we could use the measured decay constant τ_e (Supporting Materials and Methods in the Supporting Material) and the ratio C_s/C_{out} to calculate the flux rate $j_c = C_s V/C_{out}\tau_e$.

Because the intracellular fluorescence intensity F is from the dye molecules in a cell, its ratio to the outside fluorescence intensity F_{out} is not equal to C/C_{out}, which would be the case if the cell were empty like a lipid vesicle. The preexisting biological structures within the spheroplast make the accessible volume V smaller than the apparent cell volume $V_{cell.}$ To estimate the ratio $V/V_{cell} \equiv x$, we measured the maximum intracellular fluorescence intensity after a long dark period, and found it to be 0.67–0.80 of the external intensity (this ratio is x). Thus, the intracellular/extracellular concentration ratio C/C_{out} should be the corresponding fluorescence intensity ratio F/F_{out} divided by x: $C/C_{out} = F/(F_{out} \cdot x)$ (Supporting Materials and Methods). Thus, we obtain the value of $j_c = (F_s/F_{out})V_{cell}/\tau_e$, which is independent of x. From the experimental value of j_c, we used the formula $j_c = 4aDN$ to calculate the number N of the hypothetical Berg-Purcell pores (see Discussion below). We used $a = 25$Å for the size of LL37 pores measured by neutron in-plane scattering (24) and $D = 1.5 \times 10^{-6}$ cm^{2}s^{-1} for the diffusion constant of calcein in cells measured by the fluorescence correlation spectroscopy (25).

Strictly speaking, the method described above is applicable only after $C(t)$ has reached a steady state. However, since the decay rate of FRAP is faster than the changing rate of the fluorescence intensity $F(t)$, except for rare sharp transitions (such as in Fig. 2, *B1*), we also applied the same method to the presteady-state region to obtain the transient values of j_c throughout the spheroplast experiment. Fig. 2 shows the results of the LL37 experiments. We performed more than 10 runs of LL37 experiments. All were consistent with the qualitative features described above, but there were quantitative variations, as shown by the two examples in Fig. 2. The sigmoidal transition from an initial low level of intracellular fluorescence intensity to a final higher level of steady state is characteristic of all of the experiments, but the slope of the sigmoidal transition and the steady-state level varied from cell to cell (within $\sim \pm 10\%$). The duration of a spheroplast attacked by LL37 before it lost its interior phase contrast also varied (Fig. 1). Such cell-to-cell variations have also been seen in investigations of whole cells (6,9).

The same setup was used to study the effect of melittin (Fig. 3). The only difference was that the concentration of melittin delivered by the open pipe was 2 μM instead of the 6 μM used for LL37. However, the rate of calcein leakage caused by melittin was higher than that caused by LL37, since the steady-state intracellular fluorescence intensity due to melittin was 1.5–2 times that due to LL37. Superficially, this implies that melittin is the more active antimicrobial of the two. The higher activity could mean a lower threshold of the peptide/lipid ratio for pore formation (17) or a higher membrane binding affinity, or both. Otherwise the effects of both peptides are similar, indicating that they operate by the same mechanism.

DISCUSSION

The attack on whole *E. coli* cells by dye-labeled LL37 was studied by Sochacki et al. (6) using fluorescence microscopy. They observed the interruption of cell growth and the spatial distribution of the peptide while it entered the cells in real time, and found that both effects differed between septating and nonseptating cells. The attack was described as consisting of three phases. In phase 1, LL37 bound to the outer membrane. In phase 2, it spread across the periplasm to the cytoplasmic membrane. In septating cells, LL37 appeared to first concentrate at the septum region. Phase 3 involved penetration of the cytoplasmic membrane by LL37 and subsequent permeabilization to the DNA stain SYTOX Green. In our study, the spheroplasts were spherical in shape, without septa, and exhibited no cell growth in a STOP solution. Since we did not use dye-labeled AMPs, the spatial distribution of the AMPs around the spheroplast

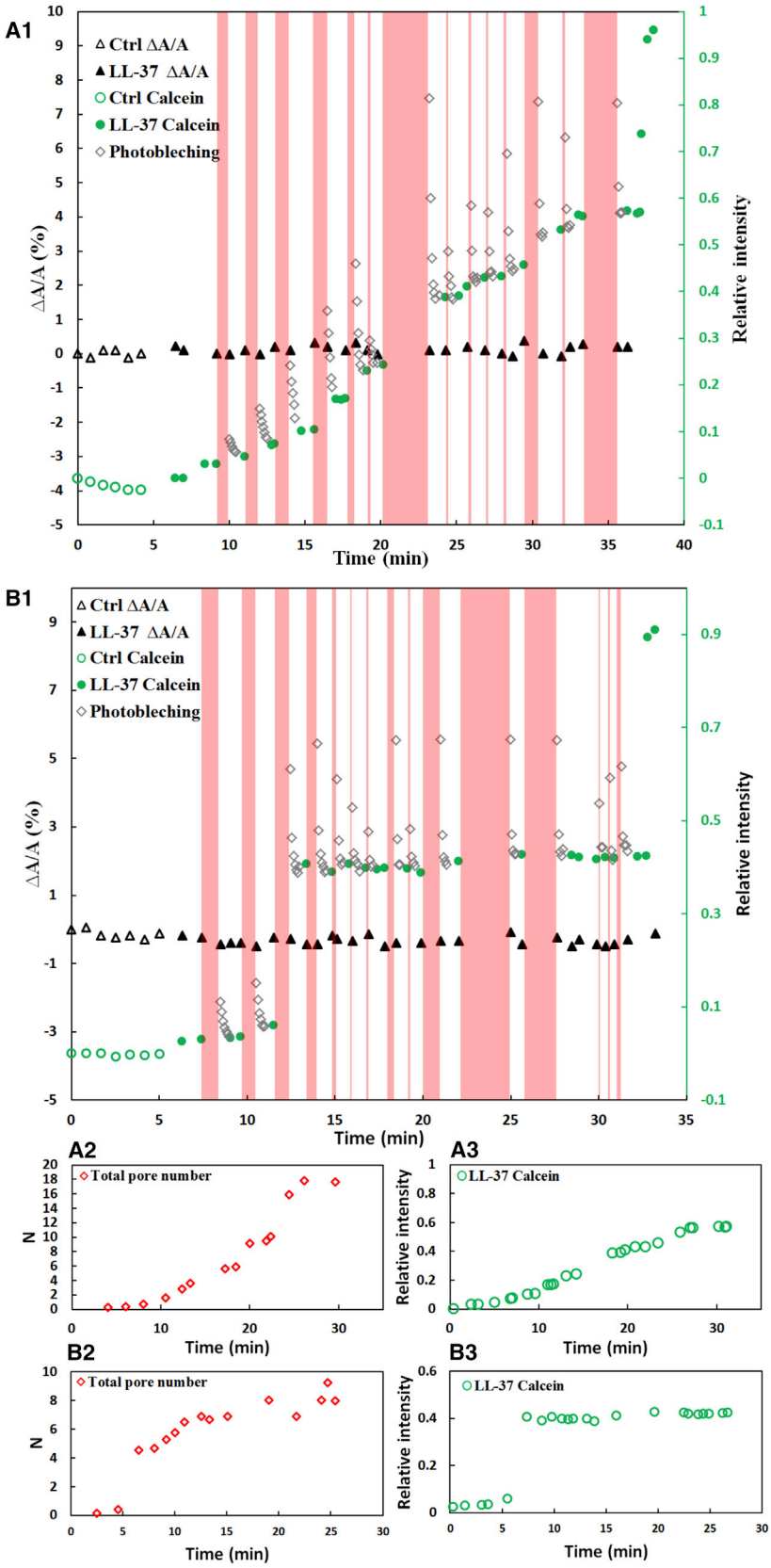

FIGURE 2 (*A* and *B*) Two complete experiments with LL37 are shown as examples. (*A1* and *B1*) The dark triangles are the fractional membrane area changes ΔA/A, which are close to zero throughout. Green symbols indicate the green fluorescence intensity inside the cell relative to outside the cell (*open green circles*, before the introduction of LL37 (control (Ctrl) period); *solid green dots*, after the introduction of LL37 at time zero), and open diamond symbols are the FRAP data. The pink stripes are the dark periods for the FRAP experiments. (*A1*) The spheroplast abruptly lost its phase contrast at ~37 min when the inside fluorescence intensity jumped to the same level as observed outside. (*A2*) A high concentration LL37 was introduced at ~33 min to cause the spheroplast to lose its phase contrast. (*A2* and *B2*) Number *N* of hypothetical Berg-Purcell pores, calculated as explained in the text. (*A3* and *B3*) The same green data as in (*A1*) and (*B1*) plotted to the same timescale as in (*A2*) and (*B2*) for comparison, showing how *N* varied as the fluorescence intensity varied.

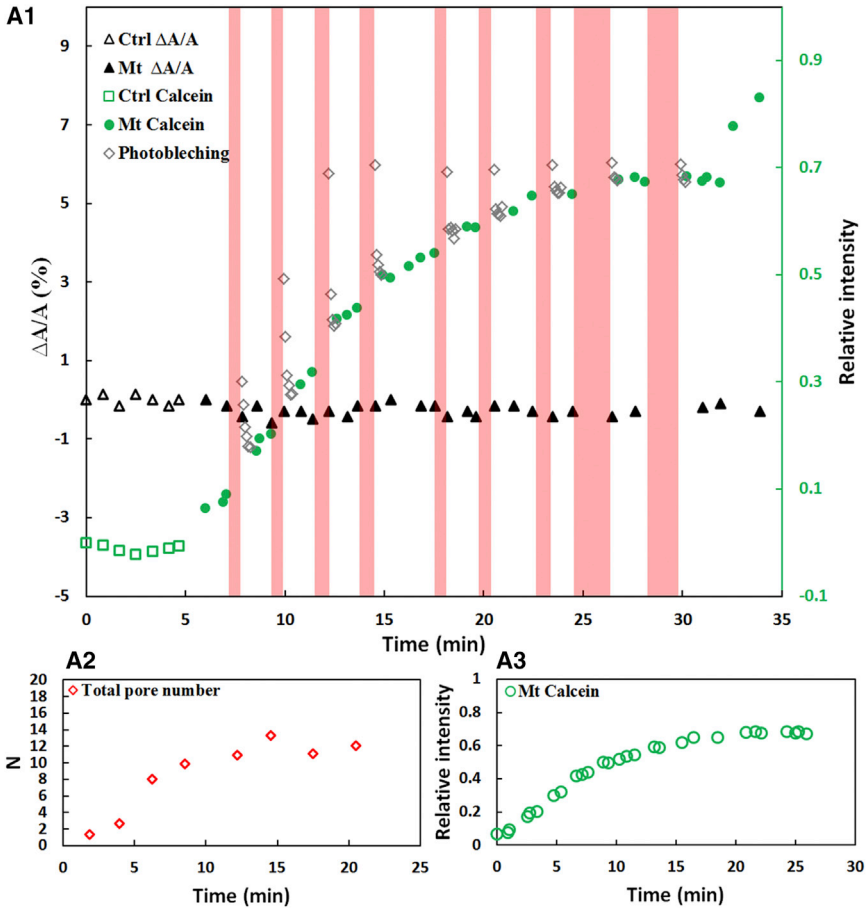

FIGURE 3 One experiment with melittin is shown as an example. (*A1*) The dark triangles are the fractional membrane area changes ΔA/A, which are close to zero throughout. Green symbols indicate the green fluorescence intensity inside the cell relative to outside the cell (*open green circles*, before the introduction of melittin (control (Ctrl) period); *solid green dots*, after the introduction of melittin at time zero), and open diamond symbols are the FRAP data. The pink stripes indicate the dark periods for the FRAP experiments. At ~33 min, the spheroplast lost its phase contrast and the fluorescence intensity began to rise to the level observed outside. At ~34 min, the spheroplast ruptured. (*A2*) Number N of hypothetical Berg-Purcell pores, calculated as explained in the text. (*A3*) The same green data as in (*A1*) plotted to the same timescale as in (*A2*) for comparison, showing how N varied as the fluorescence intensity varied.

was not visible. Instead, we measured the time-dependent intracellular and extracellular distributions of the dye molecule calcein and performed FRAP measurements. All spheroplast membranes appeared to be uniform around the cell in our experiments.

The simplest explanation for what we observed is that LL37 and melittin induced pores in the cytoplasmic membranes, and therefore we will discuss our data based on that assumption. In its original form, the Berg-Purcell formula was derived for chemoreception on the surface of a cell (23). If there is a circular receptor-binding site of radius a to which certain molecules adsorb, and assume that the site is a perfect sink for the molecules, then the diffusive flux of molecules to the site is $4aDC_{out}$ (23). If we replace the binding site by a transmembrane pore and disregard the possible friction between the pore wall and the molecular movement, then the diffusive flux through such a hypothetical Berg-Purcell pore would be $4aDC_{out}$ per pore. In other words, this would represent the diffusion flux to the mouth of the pore, which is assumed to be a perfect sink. In reality, membrane pores are as long as the membrane thickness, are not rigid, and probably are dynamical. Also, the dye molecules have a physical size. Therefore, there must be friction between the pore wall and the molecular movement. The flux through a pore must be slower than the free-diffusion flux. The fact that, if we use the theoretical formula $j_c = 4aDN$, the measured value of j_c gave a low value (~0.1) for N (the number of pores) soon after the leakage occurred indicates that the flux through a pore is at least one order of magnitude smaller than the hypothetical Berg-Purcell flux. This reduction from the free-diffusion flux rate to the experimental flux rate represents a slowdown due to the friction of the dye molecule's permeation through the pore.

Since we do not know the rate of flux through a real pore, we can only deduce a hypothetical number N that is proportional to the real number of pores in the spheroplast membrane induced by LL37 or melittin. The FRAP experiment proved that the dye concentration inside the cell was indeed maintained by diffusive fluxes through the cell membrane. The finding that N was proportional to the instantaneous intracellular fluorescence intensity under steady illumination (Figs. 2, *A2–B3*, and 3, *A2* and *A3*) shows the self-consistency of the pore model described by Eq. 1.

LL37 and melittin are both α-helical but of different lengths (37 and 26 amino acids long, respectively). Although melittin is a bee venom toxin, it has been studied as a model AMP because its general design is similar to that of AMPs

and it is active against bacteria (1,26). In studies with model membranes, melittin was shown to form toroidal pores in lipid bilayers (17,27–29). The human antimicrobial peptide LL37 has been somewhat controversial. In multilamellar samples, many investigators found LL37 in a state with its helical axis lying parallel to the plane of the bilayer (30,31). Thus, for a long time it was widely believed that LL-37 could not form pores, and therefore it was assumed to permeabilize or disintegrate membranes by a nonpore carpet mechanism (30,32,33). However, a later study found that if the multilamellar samples were overhydrated and if the peptide/lipid ratio exceeded a threshold, LL37 would turn its helical orientation to perpendicular to the bilayers, and it indeed formed pores in lipid bilayers as shown by neutron in-plane scattering (24).

There are, however, interesting differences between the membranes of spheroplasts and lipid-bilayer vesicles. In a previous study, we compared *E. coli* spheroplasts with GUVs made of *E. coli* total lipid extract (13). When a GUV was exposed to pore-forming peptides, the initial binding of peptides always expanded the membrane area of the GUV, resulting in an increased protrusion length in the aspiration micropipette (17,20,24,34,35). A simple explanation for this is that the lipid bilayer had added molecules. The subsequent pore formation caused a net water influx if, for example, sucrose and glucose were used as the solutes inside and outside the GUV, respectively, resulting in a decreased protrusion length (17,20,24,34,35). If the sucrose and glucose were exchanged, the pore formation caused a net water outflux resulting in an increased protrusion length (20). In contrast, we detected no protrusion length increase or decrease in our spheroplast experiments. On the other hand, we found that spheroplast membranes increased or decreased in area (resulting in an increased or a decreased protrusion length) in response to an aspiration pressure exactly like a GUV, albeit with a much smaller elastic area-stretching modulus compared with that of a lipid bilayer (13). Another important difference is that whereas the membrane tension of a GUV increased with decreasing external osmolality, the membrane tension of a spheroplast remained zero with varying external osmolalities (13). One possible explanation for the small area-stretching moduli and the zero membrane tension is that the bacterial membranes possess membrane reservoirs (e.g., membrane folds) (13). We do not know whether the absence of an apparent membrane area change in spheroplasts during peptide binding is due to the existence of membrane reservoirs. In view of these significant differences between spheroplast membranes and lipid bilayers, it is not clear a priori whether the pore formation by AMPs previously observed in lipid bilayers would be reproduced in spheroplasts.

This study shows that the activities of LL37 and melittin on bacterial membranes are consistent with pore formation. However, it is certainly possible to interpret the data presented here in terms of other types of peptide-induced membrane perturbations. More significantly, we discovered a new, to our knowledge, experimental parameter called the flux rate, j_c, that characterizes the AMP-induced permeability of the cytoplasmic membranes to dye molecules. This parameter has an explicit dependence on the cell volume and an implicit dependence on the AMP concentration and the size of the dye molecule. We believe that it potentially could be used for more detailed analyses of AMP mechanisms.

SUPPORTING MATERIAL

Supporting Materials and Methods and three figures are available at http://www.biophysj.org/biophysj/supplemental/S0006-3495(16)30362-9.

AUTHOR CONTRIBUTIONS

Y.S. and H.W.H. designed the research. Y.S. and T.-L.S. performed the experiments. Y.S. and H.W.H. analyzed and interpreted the results. H.W.H. wrote the article.

ACKNOWLEDGMENTS

This work was supported by the National Institutes of Health (grant GM55203) and the Robert A. Welch Foundation (grant C-0991).

REFERENCES

1. Boman, H. G., and D. Hultmark. 1987. Cell-free immunity in insects. *Annu. Rev. Microbiol.* 41:103–126.
2. Zasloff, M. 1987. Magainins, a class of antimicrobial peptides from Xenopus skin: isolation, characterization of two active forms, and partial cDNA sequence of a precursor. *Proc. Natl. Acad. Sci. USA.* 84:5449–5453.
3. Steiner, H., D. Andreu, and R. B. Merrifield. 1988. Binding and action of cecropin and cecropin analogues: antibacterial peptides from insects. *Biochim. Biophys. Acta.* 939:260–266.
4. Wade, D., A. Boman, …, R. B. Merrifield. 1990. All-D amino acid-containing channel-forming antibiotic peptides. *Proc. Natl. Acad. Sci. USA.* 87:4761–4765.
5. Boman, H. G., J. Marsh, and J. A. Goode. 1994. Antimicrobial Peptides. John Wiley and Sons, Chichester.
6. Sochacki, K. A., K. J. Barns, …, J. C. Weisshaar. 2011. Real-time attack on single Escherichia coli cells by the human antimicrobial peptide LL-37. *Proc. Natl. Acad. Sci. USA.* 108:E77–E81.
7. Rangarajan, N., S. Bakshi, and J. C. Weisshaar. 2013. Localized permeabilization of E. coli membranes by the antimicrobial peptide Cecropin A. *Biochemistry.* 52:6584–6594.
8. Barns, K. J., and J. C. Weisshaar. 2013. Real-time attack of LL-37 on single Bacillus subtilis cells. *Biochim. Biophys. Acta.* 1828:1511–1520.
9. Fantner, G. E., R. J. Barbero, …, A. M. Belcher. 2010. Kinetics of antimicrobial peptide activity measured on individual bacterial cells using high-speed atomic force microscopy. *Nat. Nanotechnol.* 5:280–285.
10. Bierbaum, G., and H. G. Sahl. 1987. Autolytic system of Staphylococcus simulans 22: influence of cationic peptides on activity of N-acetylmuramoyl-L-alanine amidase. *J. Bacteriol.* 169:5452–5458.
11. Elsbach, P., and J. Weiss. 1993. Bactericidal/permeability increasing protein and host defense against gram-negative bacteria and endotoxin. *Curr. Opin. Immunol.* 5:103–107.

12. Last, N. B., and A. D. Miranker. 2013. Common mechanism unites membrane poration by amyloid and antimicrobial peptides. *Proc. Natl. Acad. Sci. USA.* 110:6382–6387.
13. Sun, Y., T. L. Sun, and H. W. Huang. 2014. Physical properties of Escherichia coli spheroplast membranes. *Biophys. J.* 107:2082–2090.
14. Turner, J., Y. Cho, …, R. I. Lehrer. 1998. Activities of LL-37, a cathelin-associated antimicrobial peptide of human neutrophils. *Antimicrob. Agents Chemother.* 42:2206–2214.
15. Habermann, E. 1972. Bee and wasp venoms. *Science.* 177:314–322.
16. Zasloff, M. 2002. Antimicrobial peptides of multicellular organisms. *Nature.* 415:389–395.
17. Lee, M. T., T. L. Sun, …, H. W. Huang. 2013. Process of inducing pores in membranes by melittin. *Proc. Natl. Acad. Sci. USA.* 110:14243–14248.
18. Renner, L. D., and D. B. Weibel. 2011. Cardiolipin microdomains localize to negatively curved regions of Escherichia coli membranes. *Proc. Natl. Acad. Sci. USA.* 108:6264–6269.
19. Kwok, R., and E. Evans. 1981. Thermoelasticity of large lecithin bilayer vesicles. *Biophys. J.* 35:637–652.
20. Sun, Y., W. C. Hung, …, H. W. Huang. 2009. Interaction of tea catechin (-)-epigallocatechin gallate with lipid bilayers. *Biophys. J.* 96:1026–1035.
21. Sun, Y., C. C. Lee, and H. W. Huang. 2011. Adhesion and merging of lipid bilayers: a method for measuring the free energy of adhesion and hemifusion. *Biophys. J.* 100:987–995.
22. Watts, T. H., and H. M. McConnell. 1986. High-affinity fluorescent peptide binding to I-Ad in lipid membranes. *Proc. Natl. Acad. Sci. USA.* 83:9660–9664.
23. Berg, H. C., and E. M. Purcell. 1977. Physics of chemoreception. *Biophys. J.* 20:193–219.
24. Lee, C. C., Y. Sun, …, H. W. Huang. 2011. Transmembrane pores formed by human antimicrobial peptide LL-37. *Biophys. J.* 100:1688–1696.
25. Yoshida, N., M. Tamura, and M. Kinjo. 2000. Fluorescence correlation spectroscopy: a new tool for probing the microenvironment of the internal space of organelles. *Single Molecules.* 1:279–283.
26. Bucki, R., J. J. Pastore, …, P. A. Janmey. 2004. Antibacterial activities of rhodamine B-conjugated gelsolin-derived peptides compared to those of the antimicrobial peptides cathelicidin LL37, magainin II, and melittin. *Antimicrob. Agents Chemother.* 48:1526–1533.
27. Allende, D., S. A. Simon, and T. J. McIntosh. 2005. Melittin-induced bilayer leakage depends on lipid material properties: evidence for toroidal pores. *Biophys. J.* 88:1828–1837.
28. Matsuzaki, K., S. Yoneyama, and K. Miyajima. 1997. Pore formation and translocation of melittin. *Biophys. J.* 73:831–838.
29. Yang, L., T. A. Harroun, …, H. W. Huang. 2001. Barrel-stave model or toroidal model? A case study on melittin pores. *Biophys. J.* 81:1475–1485.
30. Oren, Z., J. C. Lerman, …, Y. Shai. 1999. Structure and organization of the human antimicrobial peptide LL-37 in phospholipid membranes: relevance to the molecular basis for its non-cell-selective activity. *Biochem. J.* 341:501–513.
31. Henzler Wildman, K. A., D. K. Lee, and A. Ramamoorthy. 2003. Mechanism of lipid bilayer disruption by the human antimicrobial peptide, LL-37. *Biochemistry.* 42:6545–6558.
32. Sood, R., Y. Domanov, …, P. K. Kinnunen. 2008. Binding of LL-37 to model biomembranes: insight into target vs host cell recognition. *Biochim. Biophys. Acta.* 1778:983–996.
33. Porcelli, F., R. Verardi, …, G. Veglia. 2008. NMR structure of the cathelicidin-derived human antimicrobial peptide LL-37 in dodecylphosphocholine micelles. *Biochemistry.* 47:5565–5572.
34. Longo, M. L., A. J. Waring, and D. A. Hammer. 1997. Interaction of the influenza hemagglutinin fusion peptide with lipid bilayers: area expansion and permeation. *Biophys. J.* 73:1430–1439.
35. Longo, M. L., A. J. Waring, …, D. A. Hammer. 1998. Area expansion and permeation of phospholipid membrane bilayer by influenza fusion peptides and melittin. *Langmuir.* 14:2385–2395.

Biophysical Journal, Volume *111*

Supplemental Information

Mode of Action of Antimicrobial Peptides on *E. coli* Spheroplasts

Yen Sun, Tzu-Lin Sun, and Huey W. Huang

Supplemental Information

The mode of action of antimicrobial peptides on *E. coli* spheroplasts

Yen Sun, Tzu-Lin Sun and Huey W. Huang

Department of Physics & Astronomy, Rice University, Houston Texas 77005

S1. Details of FRAP analysis

(1) Measurement of τ_e. During a dark period, the intracellular unbleached dye concentration $C(t)$ increased from the steady state value C_s to a higher value C_i when illumination resumed. Thereafter, $C(t)$ followed the kinetics:

$$C(t) - C_s = (C_i - C_s)e^{-t/\tau_e}$$

The decay constant τ_e was measured by curve fitting shown in Fig. S1.

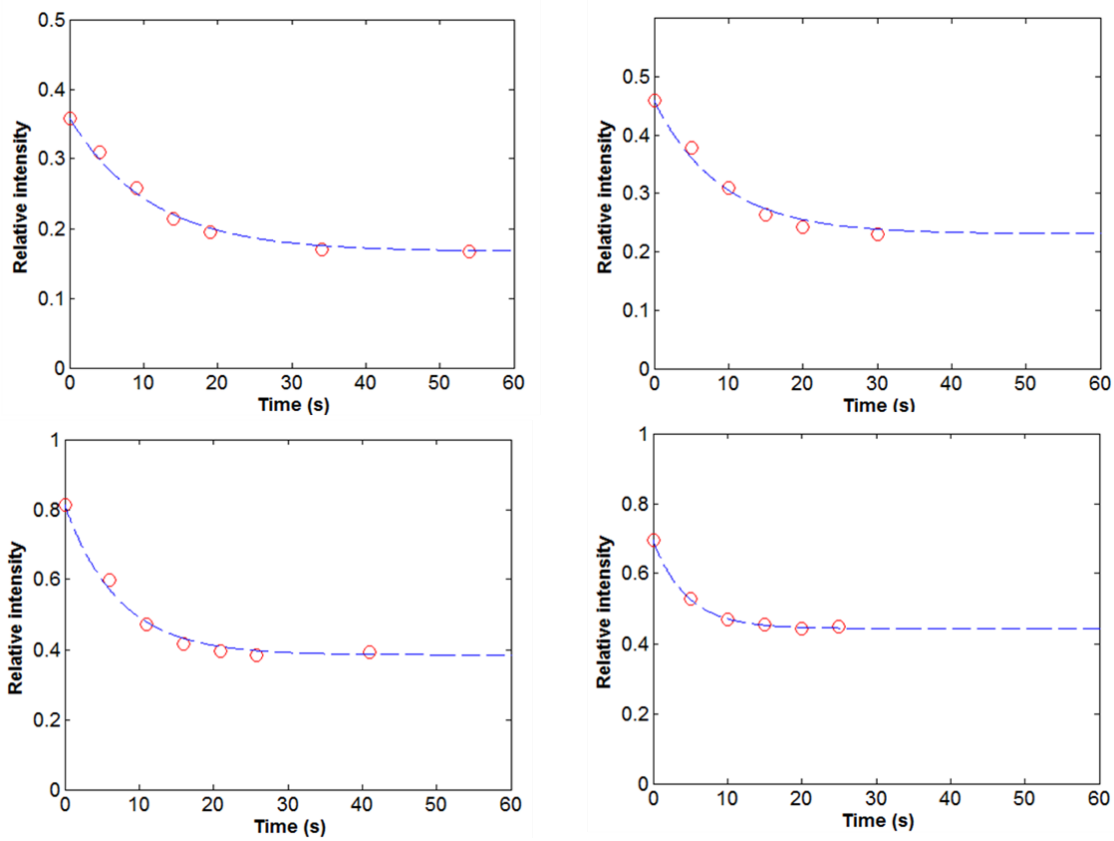

Fig. S1 Four examples of FRAP. Each was well fit by an exponential curve from which the value of τ_e was obtained.

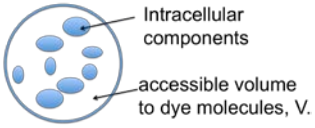

Fig. S2 Accessible volume in a cell

(2) We measured the intracellular fluorescence intensity, *F*, over the whole cell (Fig. S2). The intensity is proportional to the total number of unbleached fluorescence molecules within the measured volume. If the dye concentration *C* in the accessible volume *V* were the same as the extracellular concentration C_{out} which produced the extracellular fluorescence intensity F_{out}, the result would be

$$\frac{F}{F_{out}} = \frac{CV}{C_{out}V_{cell}} = \frac{V}{V_{cell}} \equiv x$$

Therefore, in all conditions, the correct ratio of the intracellular concentration *C* to the extracellular concentration C_{out} is obtained by the fluorescence measurement using the relation:

$$\frac{C}{C_{out}} = \frac{F}{F_{out} \cdot x}$$

Thus from $j_c = C_s V / C_{out}\tau_e$, we obtain $j_c = (F_s/F_{out})\, V_{cell}/\tau_e$.

(3) There is a second way of obtaining the value of j_c. During a dark period, there is no photobleaching, the kinetic equation for *C(t)* becomes

$$\frac{dC(t)}{dt} = -\frac{j_c}{V}C(t) + \frac{j_c}{V}C_{out}$$

During the steady state, j_c is constant, the equation can be integrated over the dark period: $C_{out} - C_i = (C_{out} - C_s)e^{-t1/\tau_j}$, where t1 is the duration of the dark period, $\frac{1}{\tau_j} = \frac{j_c}{V}$, C_s and C_i are the initial and final value of *C(t)*. Thus we can evaluate τ_j by:

$$1 - \frac{F_i}{F_{out} \cdot x} = \left(1 - \frac{F_s}{F_{out} \cdot x}\right) e^{-t1/\tau_j}$$

Then j_c is given by

$$j_c = \frac{V_{cell} \cdot x}{\tau_j}$$

The number of the hypothetical Berg-Purcell pores, N, was obtained by the formula $j_c = 4aDN$. The results obtained by two methods are compared in Fig. S3.

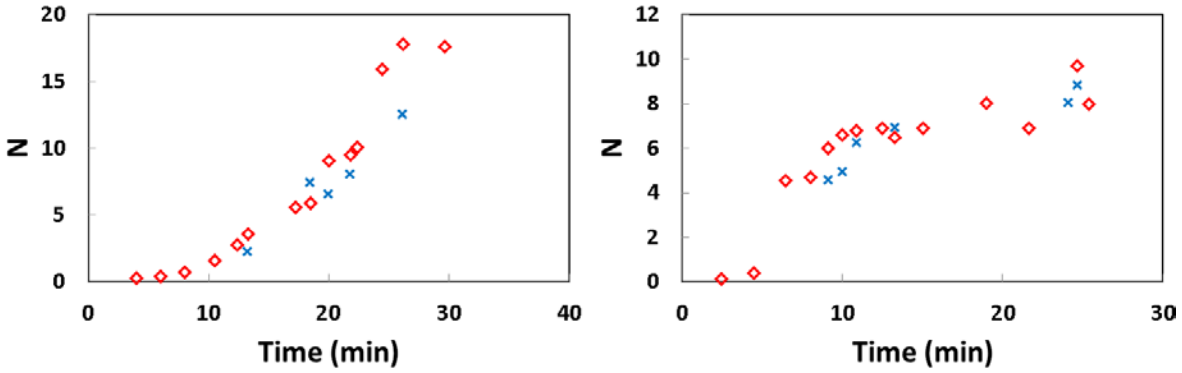

Fig. S3 The number of the hypothetical Berg-Purcell pores obtained from the two experiments shown in Fig. 2 by the first method (shown in red) and by the second method (shown in blue). The two methods yielded results close to each other.